Radiosynthesis and first preclinical evaluation of the novel 11C-labelled FAP inhibitor 11C-FAPI: A comparative study of 11C-FAPIs and [68Ga]Ga-DOTAFAPI-04 in a high–FAP-expression mouse model.

Cheng Wang (wangch628@163.com)
Department of Nuclear Medicine, Renji Hospital, School of Medicine, Shanghai Jiao Tong University
https://orcid.org/0000-0002-5312-4379

Zhoumi Hu
Department of Nuclear Medicine, Renji Hospital, School of Medicine, Shanghai Jiao Tong University

Fan Ding
Department of Nuclear Medicine, Renji Hospital, School of Medicine, Shanghai Jiao Tong University

Haitao Zhao
Department of Nuclear Medicine, Renji Hospital, School of Medicine, Shanghai Jiao Tong University

Fuqiang Du
Department of Nuclear Medicine, Renji Hospital, School of Medicine, Shanghai Jiao Tong University

Chun Lv
Department of Nuclear Medicine, Renji Hospital, School of Medicine, Shanghai Jiao Tong University

Lianghua Li
Department of Nuclear Medicine, Renji Hospital, School of Medicine, Shanghai Jiao Tong University

Gang Huang
Department of Nuclear Medicine, Renji Hospital, School of Medicine, Shanghai Jiao Tong University

Jianjun Liu
Department of Nuclear Medicine, Renji Hospital, School of Medicine, Shanghai Jiao Tong University

Research Article

Keywords: Fibroblast Activation Protein Inhibitor, Carbon-11, 11C-FAPIs, Positron Emission Tomography

Posted Date: March 23rd, 2022

DOI: https://doi.org/10.21203/rs.3.rs-1356963/v1

Abstract

Background:

^{68}Ga-labelled fibroblast activation protein inhibitors, such as [^{68}Ga]Ga-DOTA-FAPI-04 and [^{68}Ga]Ga-DOTA-FAPI-46, have been successfully applied in positron emission tomography imaging of various tumour types. To broaden the spectrum of applicable PET tracers for extended imaging studies of FAP-dependent diseases, we herein report the radiosynthesis and preclinical evaluation of two ^{11}C-labelled FAP inhibitors, ^{11}C-FAPI-01 and ^{11}C-FAPI-02.

Results:

^{11}C-FAPI-01 and ^{11}C-FAPI-02 were synthesized in over 15% radiochemical yields, with specific activities of 67 GBq/μmol and 34 GBq/μmol, respectively, at the end of synthesis and radiochemical purities greater than 99%. In U87MG tumour xenograft PET studies, the three tracers experienced higher specific uptake at the tumour site. However, because of significant differences in metabolism and clearance, [^{68}Ga]Ga-DOTA-FAPI-04 experienced high uptake in the kidney, whereas ^{11}C-FAPI-01 and ^{11}C-FAPI-02 showed high uptake in the liver and intestine. Biodistribution studies revealed significant hepatobiliary excretion of ^{11}C-FAPI-01 and ^{11}C-FAPI-02. 11C-FAPI-02 showed higher specific tumour uptake in U87MG xenografts (1.71 ± 0.08% injected dose per gram of tissue [ID/g]) than ^{11}C-FAPI-01 (1.34 ± 0.10%ID/g) and [^{68}Ga]Ga-DOTA-FAPI-04 (1.29 ± 0.04%ID/g) after 30 min p.i. In orthotopic glioma models, the uptake values were 0.07 ± 0.03% ([^{68}Ga]Ga-DOTA-FAPI-04) and 0.16 ± 0.03% (^{11}C-FAPI-02), respectively.

Conclusion:

^{11}C-FAPI-01 and ^{11}C-FAPI-02 are interesting candidates for translation to the clinic, taking advantage of the shorter half-life and physical imaging properties of C-11. The availability of ^{11}C-FAPI-01 and ^{11}C-FAPI-02 may allow extended PET studies of FAP-related diseases, such as cancer, arthritis, heart diseases, or pulmonary fibrosis.

Background

Fibroblast activation protein (FAP) is highly expressed in the stroma of a vast majority of epithelial tumours, as well as in fibrosis and rheumatoid arthritis[1]. Quinoline amide core-based FAP inhibitors (FAPIs) specifically bind to the enzymatic domain of FAP with nanomolar affinity and high selectivity[2–4]. More generally, these quinoline amide core-based FAP ligands have been conjugated with bifunctional chelating agents (BCAs), such as 1,4,7,10-tetraazacyclododecane-tetraacetic acid (DOTA) [5–7] and 1,4,7-triazacyclononane-triacetic acid (NOTA) [8, 9], for radiolabelling with various radiometals. The affinities of the inhibitors to FAP did not change considerably upon coupling of these BCAs. Labelled with the

positron emitter radionuclide ^{68}Ga, ^{18}F-Al, or ^{64}Cu complex, these tracers demonstrated high tumour-to-noise contrast ratios, fast elimination, and the successful imaging of tumour metastases [8–12]. In addition, the BCA-coupled compounds can be labelled with therapeutic nuclides, such as ^{90}Y[13, 14], ^{153}Sm [15], ^{177}Lu [16–18], ^{211}At[19], and ^{225}Ac [20], for tumour treatment. Therefore, these compounds have excellent application prospects in clinical nuclear medicine for the diagnosis and treatment of most varieties of tumours. In addition, instead of using BCAs, the glucose analogue can be directly labelled with ^{18}F and then coupled with a quinoline ring derivative by click chemistry to generate a molecular probe of the ^{18}F-labelled FAPI derivative. Preclinical biological evaluation was carried out. However, the uptake of radioactivity in the bone joints indicates that the imaging agent became defluorinated in vivo[21]. However, for the radionuclide ^{11}C, a commonly used radionuclide in the clinic, no ^{11}C-labelled compounds targeting FAP have been reported.

Herein, we report two ^{11}C-labelled small-molecule inhibitors of FAP prepared from precursors based on a quinoline amide core coupled to a 2-cyanopyrrolidine moiety: (*S*)-*N*-(2-(2-cyanopyrrolidin-1-yl)-2-oxoethyl)-6-hydroxyquinoline-4-carboxamide and (*S*)-*N*-(2-(2-cyano-4,4-difluoropyrrolidin-1-yl)-2-oxoethyl)-6-hydroxyquinoline-4-carboxamide. Then, these two precursors were conjugated with [^{11}C]CH_3I to synthesize (*S*)-*N*-(2-(2-cyanopyrrolidin-1-yl)-2-oxoethyl)-6-(methoxy-11C)quinoline-4-carboxamide (^{11}C-FAPI-01) and (*S*)-*N*-(2-(2-cyano-4,4-difluoropyrrolidin-1-yl)-2-oxoethyl)-6-(methoxy-11C)quinoline-4-carboxamide (^{11}C-FAPI-02). We report biodistribution studies and small-animal PET studies of these new ^{11}C-methylated FAPIs compared with [^{68}Ga]Ga-DOTA-FAPI-04 in nude mouse xenografts of FAP-positive tumours.

Materials And Methods

General

All chemicals and reagents were commercially obtained from Sigma–Aldrich (Shanghai, China), Bidepharm (Shanghai, China), Huayi (Changshu, China), and TanzhenBio (Nanchang, China) and used without further purification unless otherwise stated. All synthesized compounds were characterized by ^{1}H-NMR spectroscopy using a 400 MHz Bruker Avance II spectrometer. LC/MS was conducted on an Infinity Lab mass spectrometer connected to an Agilent 1260 series instrument with an Extend-C18 column (50 mm × 2.1 mm, 1.8 μm) at a UV wavelength of 254 nm. ^{11}C-CO_2 was synthesized using a medical cyclotron (HM-10, Sumitomo Heavy Industries Ltd., Tokyo, Japan) with high radiochemical purity (≥ 99%). ^{11}C-FAPI-01 and ^{11}C-FAPI-02 were automatically synthesized using a multipurpose synthesizer with a PU-2086 Plus intelligent preparation pump, a UV-2075 Plus intelligent UV/VIS detector (CFN-MPS200, Sumitomo Heavy Industries, Ltd., Japan), and a reverse-phase high-performance liquid chromatography (HPLC) column (C18-B, 250 mm × 10 mm, 5 μm, 120 Å, Morhchem Technologies Inc., USA). The probes' quality controls were analysed by HPLC (Agilent 1260 series, USA) on a C18 column (C18-B, 250 mm × 4.6 mm, 5 μm, 100 Å, Morhchem Technologies Inc., USA) with a 1260 Quat pump VL, a

1260 DAD VL detector, a 1260 Vialsampler automatic sample injector and an additional γ-detector (Eckert & Ziegler, USA). The gradient and flow rate of the water/acetonitrile mobile phase were modified for the individual products. The radioactivity was measured using a CRC®-55T activity meter (The China National Nuclear Corporation, Beijing, USA). Micro-PET/CT imaging was performed on an IRIS PET/CT system (Inviscan Imaging Systems, France).

The two precursors ((*S*)-*N*-(2-(2-cyanopyrrolidin-1-yl)-2-oxoethyl)-6-hydroxyquinoline-4-carboxamide and (*S*)-*N*-(2-(2-cyano-4,4-difluoropyrrolidin-1-yl)-2-oxoethyl)-6-hydroxyquinoline-4-carboxamide), as well as two corresponding standard compounds ((*S*)-*N*-(2-(2-cyanopyrrolidin-1-yl)-2-oxoethyl)-6-(methoxy)quinoline-4-carboxamide and (*S*)-*N*-(2-(2-cyano-4,4-difluoropyrrolidin-1-yl)-2-oxoethyl)-6-(methoxy)quinoline-4-carboxamide), were designed and synthesized by TanzhenBio and Huayi. Reagents including phosphate-buffered saline (PBS), cell culture medium, foetal bovine serum (FBS), penicillin–streptomycin solution (PS), GlutaMAX, nonessential amino acids (NEAAs), and trypsin for cell culture and subsequent experiments were obtained from Gibco (Thermo Fisher Scientific, China).

Radiosynthesis of ^{11}C-FAPI-01, ^{11}C-FAPI-02, and [^{68}Ga]Ga-DOTA-FAPI-04

The radiosynthesis of ^{11}C-FAPI-01 and ^{11}C-FAPI-02 was performed in a multipurpose synthesizer. Briefly, no-carrier-added [^{11}C]CO_2 was produced using an HM-10 cyclotron via the ^{14}N(p,α)^{11}C reaction and a gaseous target of N_2 (+ 0.5% O_2). Using the liquid method, [^{11}C]CO_2 was trapped in cold lithium aluminium hydride (LAH, -15°C in 0.1 M dry tetrahydrofuran (THF)), giving rise to the reduced product [^{11}C]CH_3OH. The THF was then evaporated off under a constant stream of N_2, and 0.5 mL of 67% HI was added to the residue containing [^{11}C]CH_3OH. The vessel was sealed and heated to 180°C before exposing the solution to a stream of nitrogen gas that bubbled the [^{11}C]CH_3I product into another − 10°C sealed vessel containing 250 µL of *N*,*N*-dimethylformamide (DMF), 1 mg of precursor and 5 µL of 5 M NaOH. The homogeneous pale-yellow solution was heated at 55°C for 2–5 min, and then the reaction mixture was quenched by 1.5 mL of HPLC solution and separated by semipreparative HPLC. The final product was trapped in a C18 Sep-Pak cartridge (WAT020515, Waters) and eluted with 0.5 mL of ethanol. After formulation with 4.5 mL of sterilized water and subsequent filtration with 0.22 µm filter membranes, the ^{11}C-labelled molecular probes were used for the next experiments. The radiosynthesis of [^{68}Ga]Ga-DOTA-FAPI-04 is illustrated in the literature[4, 7]. Briefly, 100 µg of DOTA-FAPI-04 precursor and 4 mL of a [^{68}Ga]$GaCl_3$ eluent solution (0.37 GBq in 0.05 M HCl) were mixed and adjusted to pH 4.0-4.5 with 1 mL of sodium acetate (0.25 M in water). After heating to 100°C for 10 min under constant shaking (600 rpm), the product was isolated by a C18 Sep-Pak cartridge using ethanol (0.5 mL) as the eluent. After formulation with 4.5 mL sterilized water and filtration through 0.22 µm filter membranes, [^{68}Ga]Ga-DOTA-FAPI-04 was used for the subsequent experiments, and the radiochemical purity was assessed by instant thin-layer chromatography (iTLC) (Fig. S14).

The ^{11}C-labelled compounds ^{11}C-FAPI-01 and ^{11}C-FAPI-02 were incubated in PBS at 37°C for 30, 60, 90, 120, and 150 min to measure the in vitro stability. The radiochemical purities were analysed by a radio-HPLC column (C18-B, 250 mm × 4.6 mm, 5 μm, 120 Å, Morhchem Technologies Inc., USA) (details presented in the supplemental material).

Tumour-bearing mouse model establishment

All animal experimental procedures and protocols were approved by the Institutional Animal Care and Use Committee (Renji Hospital, School of Medicine, Shanghai Jiao Tong University). For subcutaneous models, U87MG cells (2×10^6 cells in 100 μL PBS) were implanted into the right flank of female BALB/c nu/nu athymic mice to establish subcutaneous tumour xenografts. For orthotopic xenografts, U87MG cells (0.5×10^6 cells in 100 μL PBS) were transplanted into the brains of female BALB/c nude mice (4–6 weeks old). The subcutaneous and orthotopic models were ready for PET imaging three weeks after tumour cell inoculation.

PET imaging and data analyses

The products of ^{11}C-FAPI-01, ^{11}C-FAPI-02, and [^{68}Ga]Ga-DOTA-FAPI-04 were diluted or concentrated to a 74 MBq/mL. Then, 7.4 MBq (approximately 0.1 mL) of ^{11}C-FAPI-01, ^{11}C-FAPI-02 or [^{68}Ga]Ga-DOTA-FAPI-04 was intravenously injected into U87MG tumour-bearing nude mice (n = 3 for each group). For static PET imaging, the acquisition times were 30, 60, and 90 min postinjection (p.i.). For dynamic PET imaging, the duration of the scan was 60 min, and the reconstruction frames were 12×10 s, 6×30 s, and 11×300 s. Regions of interest (ROIs) in the tumour, liver, heart, kidney, brain, and lung were counted on the PET images to quantify the radioactive signals. For orthotopic xenografts, scans of ^{11}C-FAPI-02 and [^{68}Ga]Ga-DOTA-FAPI-04 were performed at 60 min p.i. All PET scans were conducted using an IRIS PET/CT system (Inviscan Imaging Systems). PET data were reconstructed using a non-scatter-corrected 3D-ordered subset expectation optimization/maximum a posteriori (OSEM3D/MAP) algorithm and subsequently analysed using Avatar 1.2 software (Pingseng China).

Biodistribution studies

In the biodistribution study, the products ^{11}C-FAPI-01 and ^{11}C-FAPI-02 were also diluted to a concentration of 74 MBq/mL. U87MG mice were injected with 3.7 MBq of each tracer and sacrificed at different times (30, 60, and 90 min p.i.; n = 3 for each time point). The main organs, including the kidney, intestine, liver, heart, lung, muscle, brain, and tumours, were isolated, weighed, and analysed. The biodistribution in the [^{68}Ga]Ga-DOTA-FAPI-04 group (3.7 MBq) with approximately 100 μg of unlabelled DOTA-FAPI-04 was also evaluated for comparison. The radioactivity of the samples was determined using an automated γ-counter (Perkin-Elmer), and the uptake of the radiotracers in different organs/tissues was calculated and presented as percent of injected dose per gram of tissue (%ID/g, mean ± SD).

Statistical analysis

Statistical analysis was performed using GraphPad software. Data are presented as the means ± SD as stated in the figure legends. $P < 0.05$ was considered statistically significant.

Results

Synthesis and Radiolabelling

Two precursor compounds, 3 and 5, and two standards compounds, 7 and 9, were synthesized by conjugation of amino and carboxyl groups (Fig. S1). The LC/MS and ^{1}HNMR spectroscopic data confirmed formation of the desired compounds (Figs. S2-S9). The radiolabelling of ^{11}C-FAPI-01 and ^{11}C-FAPI-02 is shown in Fig. 1. Using the wet method, [^{11}C]CO_2 (25 ± 3 GBq, n = 10) produced by a cyclotron was trapped in LAH (0.1 M in THF). With the addition of hydroiodic acid (w = 67%) and an increase in the reaction temperature, $^{11}CH_3I$ was generated (14 ± 2 GBq, with radiochemical yields of 56%, n = 10) and then bubbled into the yellow cold precursor DMF solution, which contained 5 μL of aqueous NaOH solution (c = 5 M). After HPLC separation and C18 column concentration, the final tracers ^{11}C-FAPI-01 (3.2 ± 0.4 GBq, n = 5) and ^{11}C-FAPI-02 (2.2 ± 0.3 GBq, n = 5) were generated in radiochemical yields of 23% and 16% (based on $^{11}CH_3I$ and without decay correction). The specific activities were 67 GBq/μmol and 34 GBq/μmol, respectively, at the end of synthesis. The total synthesis time was 30 min from the end of bombardment. The radioactive purities of these two tracers were also over 99% in PBS at 150 min, showing that the stabilities were high in vitro. The data, including the semipreparative HPLC separation conditions and stability, are shown in the supplemental material (Fig. S10-S14).

Small-animal PET studies

Tissue accumulations of the tracers were described with an ID%/g scale. In U87MG tumour-bearing nude mice, all three tracers were highly absorbed in the tumour at 30 min p.i., and the uptake decreased relatively slowly until 90 min. The accumulation of [^{68}Ga]Ga-DOTA-FAPI-04 at different times is shown in the supplemental material (Fig. S15 and Fig. S16). The tumour accumulation of ^{11}C-FAPI-01 and ^{11}C-FAPI-02 showed results similar to those of [^{68}Ga]Ga-DOTA-FAPI-04 at 30 min p.i. However, the greatest differences were observed in the liver and kidney because of the significant difference in lipid-water partition coefficients (log P) at 60 min p.i. (Fig. 2). The coronal section images at different scan times for the three tracers are shown in Fig. 3 and Fig. 4. Unlike the long-term retention of [^{68}Ga]Ga-DOTA-FAPI-04 in U87MG tumour model mice, ^{11}C-FAPI-01 and ^{11}C-FAPI-02 showed rapid elimination in the kidney but long-term retention in the liver and intestine. For ^{11}C-FAPI-02, 60-min dynamic PET was performed in U87MG tumour xenografts. The tumour accumulation of ^{11}C-FAPI-02 was rapid. In contrast, sudden elimination form the heart, kidney, and liver was observed. Moreover, uptake in the intestine was also high (Fig. 5). Regarding ^{11}C-FAPI-02 PET in U87MG tumour xenografts, tumour accumulation was rapid. Slightly increased tumour uptake was observed from 30 min to 60 min, and then constant uptake occurred between 60 and 90 min. In the U87 orthotopic xenograft glioma model small-animal PET study, ^{11}C-FAPI-02 accumulated in the tumour at significantly higher levels than [^{68}Ga]Ga-DOTA-FAPI-04 (Fig. 6).

Organ distribution in U87MG tumour xenografts

The biodistribution of the three tracers in U87MG tumour xenografts was determined by ex vivo counting in tissues collected 30, 60, and 90 min after injection (Table 1). At 30, 60, 90 min p.i., [^{68}Ga]Ga-DOTA-FAPI-04 accumulated mainly in the tumour (1.29 ± 0.04, 0.60 ± 0.09 and 0.19 ± 0.05% ID/g) and kidney (28.37 ± 4.67, 1.54 ± 0.38 and 0.46 ± 0.06% ID/g), and the tumour-to-muscle (T/M) ratio was 1.16 ± 0.25, 2.53 ± 0.38 and 4.74 ± 0.07, respectively. Other organs demonstrated low nonspecific binding that quickly decreased, resulting in a low background signal and favourable tumour-to-background ratios.

Table 1
the distribution of three molecular probes in different organs.

Tracers	[68Ga]Ga-DOTA-FAPI-04			^{11}C-FAPI-01			^{11}C-FAPI-02		
Time(min)	30	60	120	30	60	90	30	60	90
Tumor	1.29 ± 0.04	0.60 ± 0.09	0.19 ± 0.05	1.34 ± 0.10	0.15 ± 0.01	0.02 ± 0.00	1.71 ± 0.08	0.62 ± 0.06	0.18 ± 0.02
Kidney	28.37 ± 4.67	1.54 ± 0.38	0.46 ± 0.06	1.28 ± 0.06	0.17 ± 0.02	0.03 ± 0.00	1.84 ± 0.01	0.48 ± 0.02	0.13 ± 0.02
Intestine	1.40 ± 0.03	0.67 ± 0.05	0.27 ± 0.02	4.95 ± 0.31	2.72 ± 0.45	0.67 ± 0.02	5.08 ± 0.24	2.63 ± 0.28	1.10 ± 0.25
Liver	2.08 ± 0.05	0.90 ± 0.07	0.22 ± 0.03	7.20 ± 1.71	0.24 ± 0.03	0.06 ± 0.00	2.87 ± 0.12	1.00 ± 0.05	0.29 ± 0.02
Heart	2.86 ± 0.09	0.43 ± 0.03	0.08 ± 0.01	0.59 ± 0.01	0.06 ± 0.01	0.01 ± 0.00	0.78 ± 0.10	0.26 ± 0.01	0.07 ± 0.01
Lung	1.69 ± 0.07	0.27 ± 0.01	0.10 ± 0.01	0.56 ± 0.08	0.05 ± 0.01	0.01 ± 0.00	0.65 ± 0.02	0.25 ± 0.03	0.06 ± 0.01
Muscle	1.15 ± 0.28	0.23 ± 0.01	0.04 ± 0.01	0.42 ± 0.04	0.06 ± 0.01	0.01 ± 0.00	0.74 ± 0.03	0.20 ± 0.01	0.04 ± 0.00
Brain	0.52 ± 0.03	0.09 ± 0.02	0.02 ± 0.01	0.18 ± 0.02	0.02 ± 0.00	0.00 ± 0.00	0.16 ± 0.01	0.07 ± 0.03	0.02 ± 0.01

At 30, 60, 90 min p.i., ^{11}C-FAPI-01 accumulated mainly in the tumour (1.34 ± 0.10, 0.15 ± 0.01 and 0.02 ± 0.00%ID/g), kidney (1.28 ± 0.06, 0.17 ± 0.02 and 0.03 ± 0.00%ID/g) and liver (7.20 ± 1.27, 0.24 ± 0.03 and 0.06 ± 0.00%ID/g), and the T/M ratio was 3.19 ± 0.06, 2.26 ± 0.25 and 2.00 ± 0.00, respectively (Fig. 7). The higher uptake in the liver and intestine demonstrated a slow decrease and clearance, resulting in a higher background signal but a more favourable T/M ratio than [^{68}Ga]Ga-DOTA-FAPI-04 (Fig. 7).

At 30, 60, 90 min p.i., ^{11}C-FAPI-02 accumulated mainly in the tumour (1.71 ± 0.08, 0.62 ± 0.06 and 0.18 ± 0.02%ID/g), kidney (1.84 ± 0.01, 0.48 ± 0.02 and 0.13 ± 0.02%ID/g) and liver (2.87 ± 0.12, 1.00 ± 0.05 and 0.29 ± 0.02%ID/g). The T/M ratios were 2.30 ± 0.32, 3.10 ± 0.14 and 4.50 ± 0.50, respectively (Fig. 7). The

higher uptake of ^{11}C-FAPI-02 in the liver and intestine was similar to that of ^{11}C-FAPI-01. Additionally, slowly decreasing clearance resulted in a higher background signal but also a more favourable T/M ratio than those of [^{68}Ga]Ga-DOTA-FAPI-04.

Discussion

Based on quinoline amide core-based FAP inhibitors, many macrocyclic species, such as DOTA-, NOTA-conjugated chelation reagents, have been developed[22]. However, these bifunctional chelator-coupled compounds have been labelled with metal radionuclides, such as ^{68}Ga and Al^{18}F for PET imaging, ^{99m}Tc for SPECT imaging, and ^{177}Lu, ^{225}Ac, and ^{223}Ra for internal exposure treatment in the clinic. Among the imaging tracers, [^{68}Ga]Ga-DOTA-FAPI-04 showed excellent pharmacokinetic mechanisms for clinical use in a variety of tumours. As derivatives of small-molecule inhibitors, these tracers showed quick metabolism and clearance from the body, resulting in excellent T/NT values and lower total-body effective doses. Due to the rapid biological half-lives and the short physical half-life of ^{68}Ga (67.7 min), [^{68}Ga]Ga-DOTA-FAPI-04 is the most studied and reported PET molecular imaging probe.

In this research, we chose the exact inhibitor ((S)-*N*-(2-(2-cyano-4,4-difluoropyrrolidin-1-yl)-2-oxoethyl)-6-(methoxy) quinoline-4-carboxamide, IC_{50} = 8.5 ± 0.9 nM[3]) of FAP and its analogue (S)-*N*-(2-(2-cyanopyrrolidin-1-yl)-2-oxoethyl)-6-(methoxy) quinoline-4-carboxamide as the standard compounds, labelled them with the PET radionuclide ^{11}C (half-life, 20.4 min), and examined the potential of the tracers as PET molecular imaging probes in tumour model mice.

First, the precursors of these inhibitors were synthesized and labelled with $^{11}CH_3I$ or $^{11}CH_3OTf$ in several organic solvents, such as DMF, DMSO, THF, and acetone, containing different bases, such as NaOH, NaH, and triethylamine. The reaction temperature was controlled at room temperature, 55°C or 80°C. Finally, the optimal reaction conditions were 1 mg of precursor, $^{11}CH_3I$ in 250 μL of DMF containing 5 μL of NaOH (5 M) at 55°C, resulting in radiochemical yields of 23% (^{11}C-FAPI-01) and 16% (^{11}C-FAPI-02). The final products were identified by HPLC analysis with a radio detector method after HPLC and solid-phase extraction (SPE) using anhydrous ethanol as the solvent and an SPE C-18 cartridge as the solid-phase column, respectively.

The significant differences in log P among the three radioprobes reflected the different metabolism and clearance pathways. The higher water solubility of [^{68}Ga]Ga-DOTA-FAPI-04 (log P = 0.25) resulted in high kidney clearance, and the higher lipid solubility of ^{11}C-FAPI-01 (log P = 0.63) and ^{11}C-FAPI-02 (log P = 1.27) resulted in good hepatobiliary clearance. These results were confirmed by small-animal PET/CT imaging and the organ distributions in the model mice.

As previously described, [^{68}Ga]Ga-DOTA-FAPI-04 was rapidly distributed in all organs of the model mice in 30 min. Because of the rapid distribution, the T/K ratios showed a consistent increase from 0.04 ± 0.01

(30 min p.i.) to 0.41 ± 0.06 ID%/g (after 90 min p.i.), and the corresponding tumour/muscle (T/M) ratios changed from 1.16 ± 0.25 to 4.74 ± 0.07.

Similar to the [^{68}Ga]Ga-DOTA-FAPI-04 small-animal imaging and organ distribution in U87MG cells, both ^{11}C-FAPI-01 and ^{11}C-FAPI-02 were rapidly distributed in all organs of the model mice in 30 min. The T/K ratios for these two probes were 1.05 ± 0.03 and 0.93 ± 0.04 at 60 and 90 min p.i., and the T/K radios were 0.89 ± 0.05 and 0.67 ± 0.01 and 1.29 ± 0.07 and 1.39 ± 0.06, respectively. However, the greatest difference was that the organ with the highest uptake was the kidney for the previous tracer but the liver for ^{11}C-FAPI-01 and ^{11}C-FAPI-02. Both ^{11}C-FAPI-01 and ^{11}C-FAPI-02 accumulated rapidly in the tumour and other organs in 30 min and resulted in higher T/M (3.19 ± 0.06 in ^{11}C-FAPI-01 and 2.30 ± 0.02 in ^{11}C-FAPI-02). As the liver is the major organ that metabolizes most drugs, the T/L ratios were examined. For ^{11}C-FAPI-01, the ratios at 30, 60, 90 min p.i. were 0.19 ± 0.03, 0.63 ± 0.04, and 0.34 ± 0.06, respectively. For ^{11}C-FAPI-02, the ratios were 0.60 ± 0.03, 0.62 ± 0.03 and 0.62 ± 0.03. Significant disparities in the liver and kidney were observed because of the differences in drug metabolism and clearance. As a difference between [^{68}Ga]Ga-DOTA-FAPI-04 and ^{68}Ga-FAPI-02, due to the existence of difluorine atoms in the proline derivative residues of ^{11}C-FAPI-02, the lipid solubility was enhanced compared with that of ^{11}C-FAPI-01, resulting in rapid accumulation and slow clearance in organs, especially in tumours.

Due to the enhanced lipid solubility of ^{11}C-FAPI-02, the in vivo tumour accumulation efficacy of ^{11}C-FAPI-02 and [^{68}Ga]Ga-DOTA-FAPI-04 was evaluated in a mouse model of orthotopic glioma. An interesting finding was that in contrast to the radioactive accumulations in the brain of U87MG tumour xenografts and in the orthotopic model, no differences were observed between the two at 60 min p.i. except for with ^{11}C-FAPI-02. A significant difference in the brain was observed at 60 min p.i. This means that the ^{11}C-labelled tracers can more easily cross the blood–brain barrier and image the glioma in the brain earlier than [^{68}Ga]Ga-DOTA-FAPI-04. Further studies of this observed phenomenon are ongoing.

Conclusion

The ^{11}C-labelled FAP inhibitors ^{11}C-FAPI-01 and ^{11}C-FAPI-02 experience improved tumour uptake and longer tumour retention times than [^{68}Ga]Ga-DOTA-FAPI-04. These two ^{11}C-labelled FAPIs are interesting candidates for translation to the clinic, taking advantage of the shorter half-life and physical imaging properties of C-11. The availability of ^{11}C-FAPI-01 and ^{11}C-FAPI-02 may allow extended PET studies of FAP-related diseases, such as cancer, arthritis, heart diseases, or pulmonary fibrosis.

Abbreviations

BCAs
Bifunctional chelating agents
CT
Computed tomography

DMF
N,*N*-dimethylformamide
DMSO
Dimethyl sulfoxide
DOTA
1,4,7,10-Tetraazacyclododecane-1,4,7,10-tetraacetic acid
FAP
Fibroblast activation protein
FAPI
Fibroblast activation protein inhibitors
FBS
Foetal bovine serum
HPLC
High performance liquid chromatography
%ID/g
Percent injected dose per gram of tissue
ITLC
Instant thin layer chromatography
LAH
Lithium aluminium hydride
LC/MS
Liquid chromatography/mass spectroscopy
MBq
Megabecquerel
NEAAs
Nonessential amino acids
NOTA
1,4,7-Triazacyclononane-1,4,7-triacetic acid
PBS
Phosphate-buffered saline
PET
Positron emission tomography
PS
Penicillin–streptomycin solution
RCY
Radiochemical yield
Rf
Retention factor
SPECT
Single-photon emission computed tomography

TAC
Time activity curve
THF
Tetrahydrofuran
T/K
Tumour-to-kidney
T/L
Tumour-to-liver
TLC
Thin layer chromatography
T/M
Tumour-to-muscle
T/NT
Tumour-to-non target

Declarations

Acknowledgements

We gratefully appreciate all the chemists, nurses and technicians from the Department of Nuclear Medicine, Renji Hospital, School of Medicine, Shanghai Jiao Tong University, for their contributions to the tracer administration and PET/CT imaging.

Fundings

This work was funded by the National Key R&D Program of China (Grant number 2021YFF0701900 and 2020YFA0909000) and the Interdisciplinary Program of Shanghai Jiao Tong University (Grant number ZH2018QNB20).

Availability of data and materials

All data generated or analysed during this study are included in this published article and its supplementary information files.

Author information

Affiliations

1. Department of Nuclear Medicine, Renji Hospital, School of Medicine, Shanghai Jiao Tong University, 1630 Dongfang Rd, Shanghai 200127, China

Cheng Wang, Zhoumi Hu, Fan Ding, Haitao Zhao, Fuqiang Du, Chun Lv, Lianghua Li, Gang Huang & Jianjun Liu

2. Shanghai Key Laboratory of Molecular Imaging, Shanghai University of Medicine and Health Sciences, Shanghai, China

Gang Huang

Contributions

CW, GH and JL conceived and designed this research. CW and ZH were responsible for all the experiments, data collection and analysis and wrote the manuscript. Fan D, H Z, Fuqiang D, and CL were involved in the preparation of the radionuclide and radiopharmaceuticals and took part in most of the animal experiments. LL was responsible for the small-animal image analysis. All the authors participated in the revision of the article. All authors read and approved the final manuscript.

*** First authors, contributed equally to this work**

Cheng Wang, Email: wangch628@163.com

Zhoumi Hu, Email: huzhoumi@hotmail.com

† Corresponding Authors:

Cheng Wang, PhD

E-mail: wangch628@163.com.

ORCID ID: 0000-0002-5312-4379

Prof. Gang Huang

E-mail: huanggang2802@163.com.

Prof. Jianjun Liu

E-mail: nuclearj@163.com.

Ethics declarations

Ethics approval

Micro-PET imaging experiments and biodistribution studies were performed in mice according to a protocol approved by the Renji Hospital Institutional Animal Care and Use Committee. All applicable international, national, and institutional guidelines for the care and use of animals were followed. All

methods were carried out in accordance with relevant guidelines and regulations. And the study was carried out in compliance with the ARRIVE guidelines.

Conflict of interest

The authors declare that they have no competing interests.

Consent for publication

Not applicable.

References

1. Kalluri R. The biology and function of fibroblasts in cancer. Nat Rev Cancer. 2016;16:582–98. doi:10.1038/nrc.2016.73.
2. Jansen K, Heirbaut L, Cheng JD, Joossens J, Ryabtsova O, Cos P, et al. Selective Inhibitors of Fibroblast Activation Protein (FAP) with a (4-Quinolinoyl)-glycyl-2-cyanopyrrolidine Scaffold. ACS Med Chem Lett. 2013;4:491–6. doi:10.1021/ml300410d.
3. Jansen K, Heirbaut L, Verkerk R, Cheng JD, Joossens J, Cos P, et al. Extended Structure–Activity Relationship and Pharmacokinetic Investigation of (4-Quinolinoyl)glycyl-2-cyanopyrrolidine Inhibitors of Fibroblast Activation Protein (FAP). J Med Chem. 2014;57:3053–74. doi:10.1021/jm500031w.
4. Lindner T, Loktev A, Altmann A, Giesel F, Kratochwil C, Debus J, et al. Development of Quinoline-Based Theranostic Ligands for the Targeting of Fibroblast Activation Protein. J Nucl Med. 2018;59:1415–22. doi:10.2967/jnumed.118.210443.
5. Giesel FL, Kratochwil C, Lindner T, Marschalek MM, Loktev A, Lehnert W, et al. ^{68}Ga-FAPI PET/CT: Biodistribution and Preliminary Dosimetry Estimate of 2 DOTA-Containing FAP-Targeting Agents in Patients with Various Cancers. J Nucl Med. 2019;60:386–92. doi:10.2967/jnumed.118.215913.
6. Kratochwil C, Flechsig P, Lindner T, Abderrahim L, Altmann A, Mier W, et al. ^{68}Ga-FAPI PET/CT: Tracer Uptake in 28 Different Kinds of Cancer. J Nucl Med. 2019;60:801–5. doi:10.2967/jnumed.119.227967.
7. Loktev A, Lindner T, Mier W, Debus J, Altmann A, Jäger D, et al. A Tumor-Imaging Method Targeting Cancer-Associated Fibroblasts. J Nucl Med. 2018;59:1423–9. doi:10.2967/jnumed.118.210435.
8. Wang S, Zhou X, Xu X, Ding J, Liu S, Hou X, et al. Clinical translational evaluation of Al^{18}F-NOTA-FAPI for fibroblast activation protein-targeted tumour imaging. Eur J Nucl Med Mol Imaging. 2021;48:4259–71. doi:10.1007/s00259-021-05470-5.
9. Giesel FL, Adeberg S, Syed M, Lindner T, Jimenez-Franco LD, Mavriopoulou E, et al. FAPI-74 PET/CT Using Either ^{18}F-AlF or Cold-Kit ^{68}Ga Labeling: Biodistribution, Radiation Dosimetry, and Tumor Delineation in Lung Cancer Patients. J Nucl Med. 2021;62:201–7. doi:10.2967/jnumed.120.245084.
10. Chen HJ, Pang YZ, Wu JX, Zhao L, Hao B, Wu J, et al. Comparison of Ga-68 Ga-DOTA-FAPI-04 and F-18 FDG PET/CT for the diagnosis of primary and metastatic lesions in patients with various types of

cancer. Eur J Nucl Med Mol Imaging. 2020;47:1820–32. doi:10.1007/s00259-020-04769-z.

11. Watabe T, Liu Y, Kaneda-Nakashima K, Shirakami Y, Lindner T, Ooe K, et al. Theranostics Targeting Fibroblast Activation Protein in the Tumor Stroma: ^{64}Cu- and ^{225}Ac-Labeled FAPI-04 in Pancreatic Cancer Xenograft Mouse Models. J Nucl Med. 2020;61:563–9. doi:10.2967/jnumed.119.233122.
12. Archibald SJ, Allott L. The aluminium-[^{18}F]fluoride revolution: simple radiochemistry with a big impact for radiolabelled biomolecules. EJNMMI Radiopharmacy and Chemistry. 2021;6:30. doi:10.1186/s41181-021-00141-0.
13. Ferdinandus J, Fragoso Costa P, Kessler L, Weber M, Hirmas N, Kostbade K, et al. Initial clinical experience with ^{90}Y-FAPI-46 radioligand therapy for advanced stage solid tumors: a case series of nine patients. J Nucl Med. 2021. doi:10.2967/jnumed.121.262468.
14. Rathke H, Fuxius S, Giesel FL, Lindner T, Debus J, Haberkorn U, et al. Two Tumors, One Target Preliminary Experience With Y-90-FAPI Therapy in a Patient With Metastasized Breast and Colorectal Cancer. Clin Nucl Med. 2021;46:842–4. doi:10.1097/rlu.0000000000003842.
15. Kratochwil C, Giesel FL, Rathke H, Fink R, Dendl K, Debus J, et al. Sm-153 Samarium-labeled FAPI-46 radioligand therapy in a patient with lung metastases of a sarcoma. Eur J Nucl Med Mol Imaging. 2021;48:3011–3. doi:10.1007/s00259-021-05273-8.
16. Kuyumcu S, Kovan B, Sanli Y, Buyukkaya F, Simsek DH, Ozkan ZG, et al. Safety of Fibroblast Activation Protein-Targeted Radionuclide Therapy by a Low-Dose Dosimetric Approach Using Lu-177-FAPI04. Clin Nucl Med. 2021;46:641–6. doi:10.1097/rlu.0000000000003667.
17. Fu KL, Pang YZ, Zhao L, Lin LM, Wu H, Sun L, et al. FAP-targeted radionuclide therapy with Lu-177 Lu-FAPI-46 in metastatic nasopharyngeal carcinoma. Eur J Nucl Med Mol Imaging. 2021. doi:10.1007/s00259-021-05634-3.
18. Ballal S, Yadav MP, Kramer V, Moon ES, Roesch F, Tripathi M, et al. A theranostic approach of Ga-68 Ga-DOTA.SA.FAPi PET/CT-guided Lu-177 Lu-DOTA.SA.FAPi radionuclide therapy in an end-stage breast cancer patient: new frontier in targeted radionuclide therapy. Eur J Nucl Med Mol Imaging. 2021;48:942–4. doi:10.1007/s00259-020-04990-w.
19. Ma H, Li F, Shen G, Pan L, Liu W, Liang R, et al. In vitro and in vivo evaluation of 211At-labeled fibroblast activation protein inhibitor for glioma treatment. Bioorg Med Chem. 1800;55:116600. doi:10.1016/j.bmc.2021.116600.
20. Liu YW, Watabe T, Kaneda-Nakashima K, Shirakami Y, Naka S, Ooe K, et al. Fibroblast activation protein targeted therapy using Lu-177 FAPI-46 compared with Ac-225 FAPI-46 in a pancreatic cancer model. Eur J Nucl Med Mol Imaging. doi:10.1007/s00259-021-05554-2.
21. Toms J, Kogler J, Maschauer S, Daniel C, Schmidkonz C, Kuwert T, et al. Targeting Fibroblast Activation Protein: Radiosynthesis and Preclinical Evaluation of an < sup > 18</sup > F-Labeled FAP Inhibitor. J Nucl Med. 2020;61:1806–13. doi:10.2967/jnumed.120.242958.
22. Windisch P, Zwahlen DR, Giesel FL, Scholz E, Lugenbiel P, Debus J, et al. Clinical results of fibroblast activation protein (FAP) specific PET for non-malignant indications: systematic review. EJNMMI Res. 2021;11:18. doi:10.1186/s13550-021-00761-2.

Figures

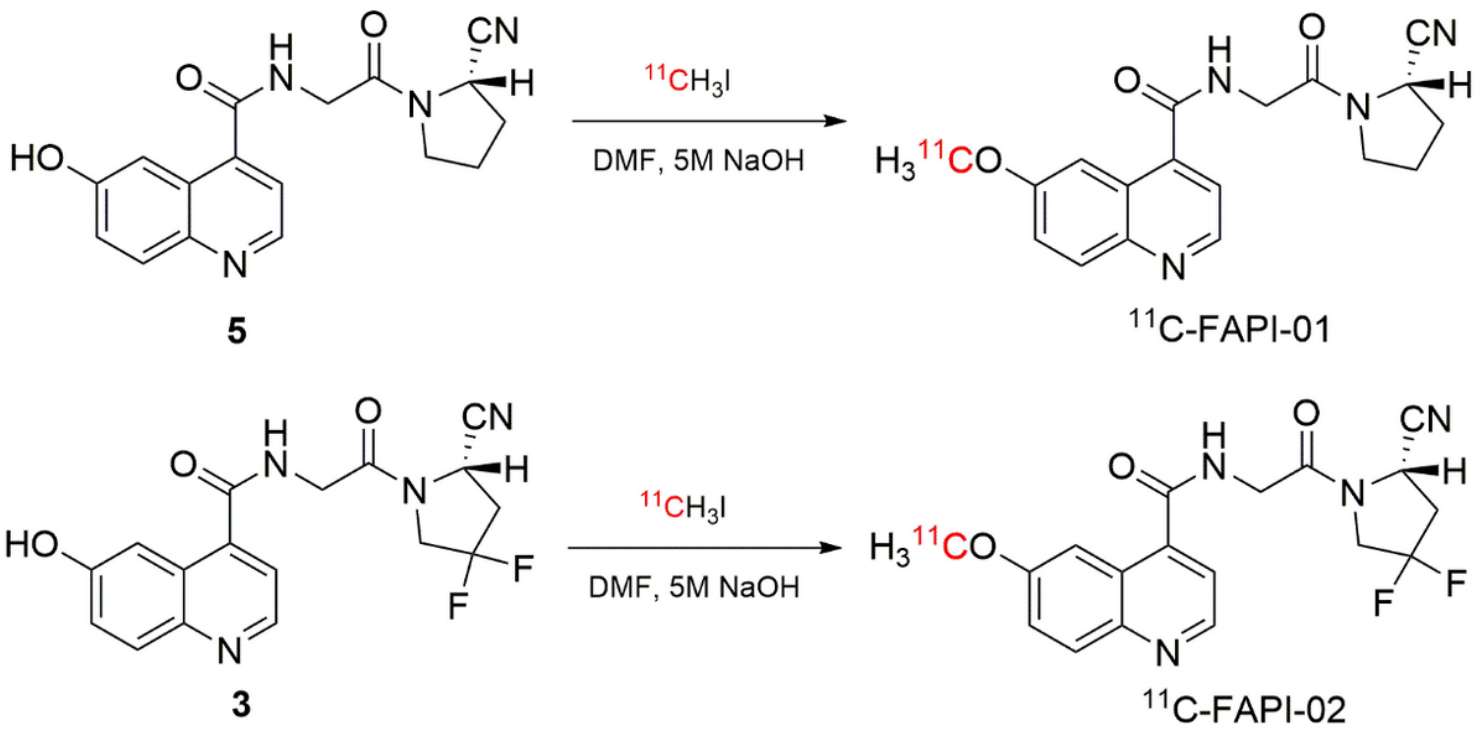

Figure 1

The radiolabeling of ^{11}C-FAPI-01 and ^{11}C-FAPI-02

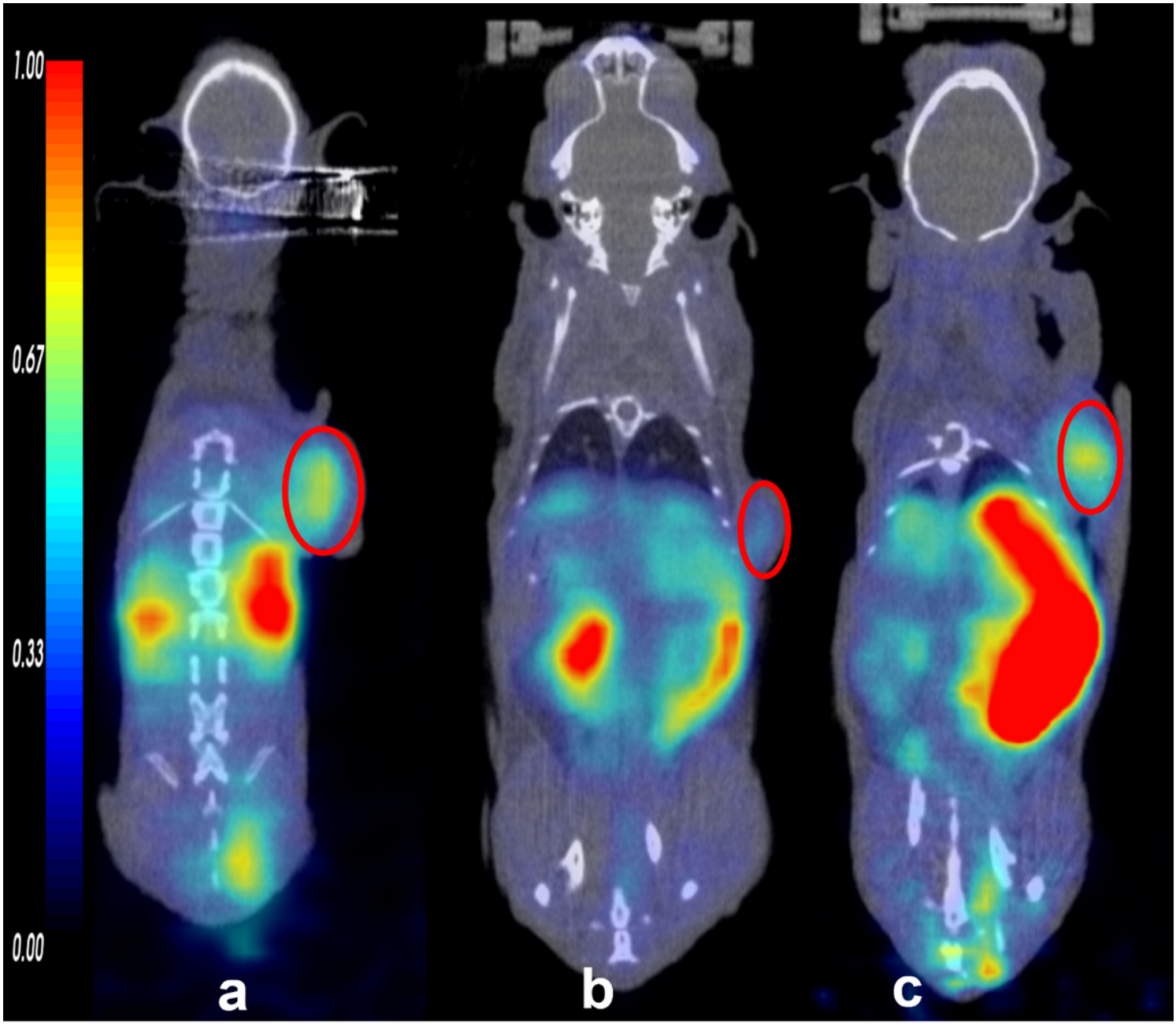

Figure 2

The small animal PET/CT imaging of the tracers [^{68}Ga]Ga-DOTA-FAPI-04 (**a**), ^{11}C-FAPI-01(**b**), and ^{11}C-FAPI-02(**c**) at 60min. And the tumor was indicated by the red circle.

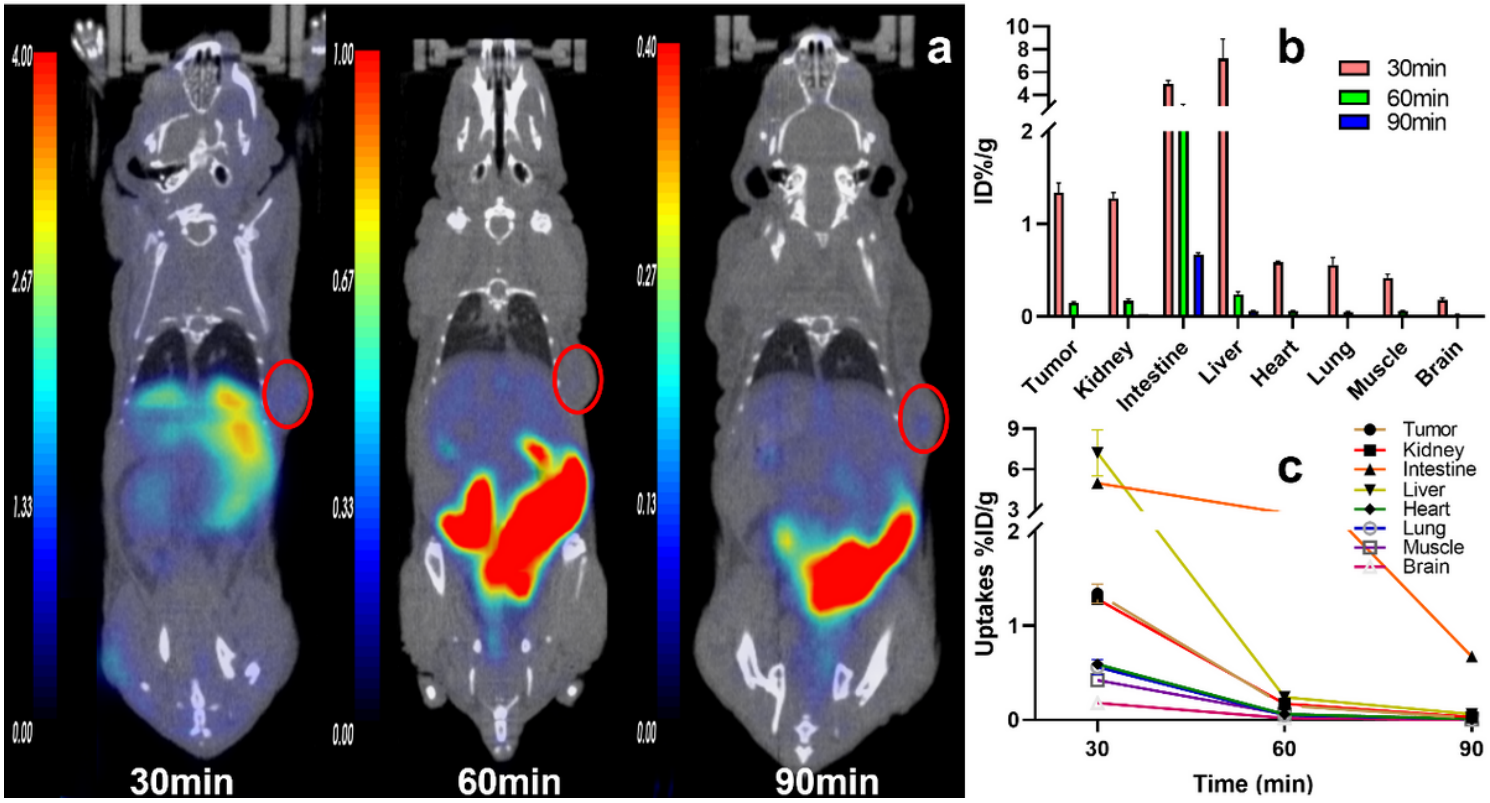

Figure 3

The Representative static PET imaging and distribution of ^{11}C-FAPI-01, **a**: The Representative static PET imaging of ^{11}C-FAPI-01 at 30, 60, 90min in U87MG tumor-bearing nude mice. And the tumor was indicated by the red circle; **b**: The organs or tissues uptakes of ^{11}C-FAPI-01 in U87MG tumor-bearing nude mice at 30, 60, 90min; **c**: the time-active-curve (TAC) of ^{11}C-FAPI-01 at 30, 60, 90min.

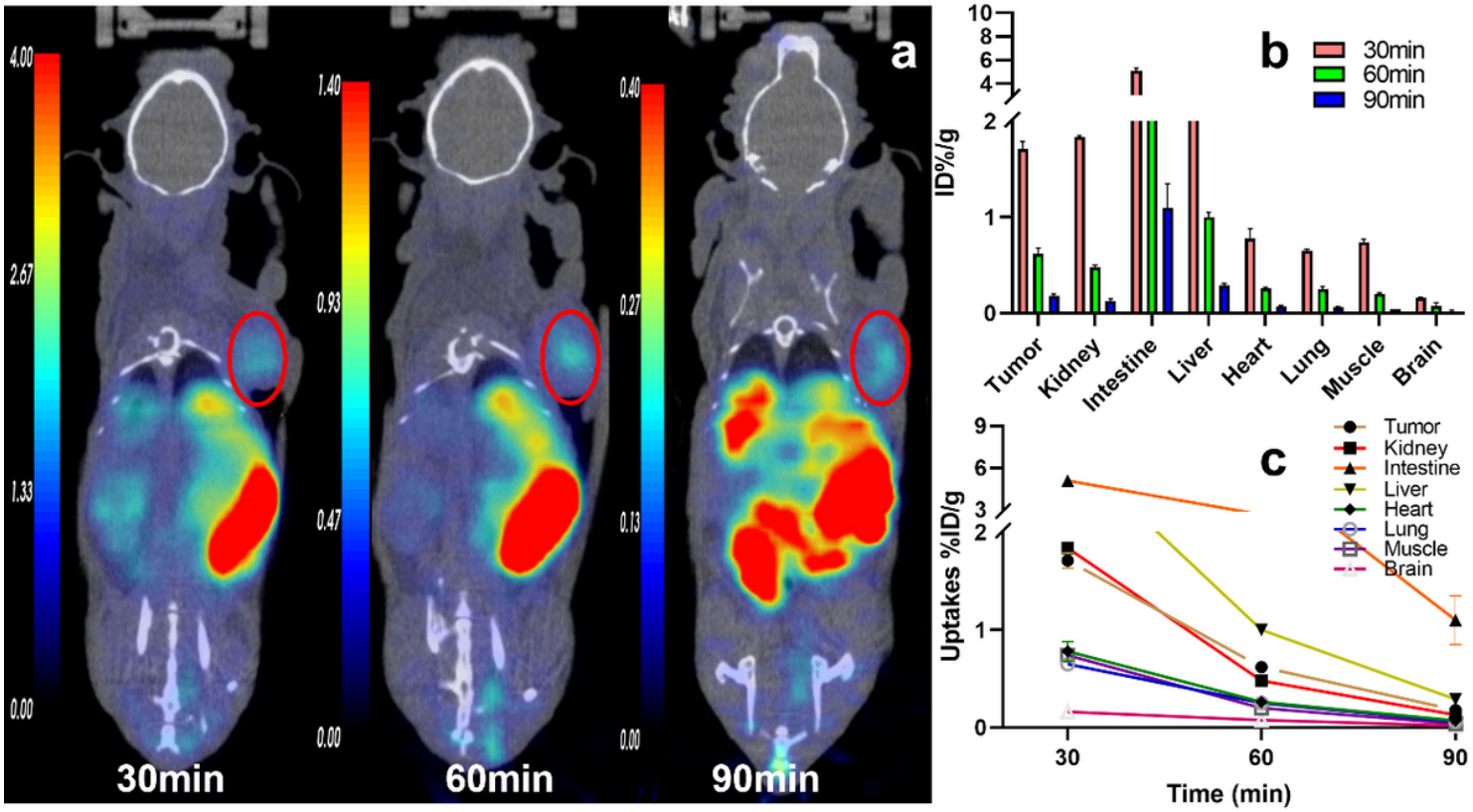

Figure 4

The Representative static PET imaging and distribution of ^{11}C-FAPI-02, **a**: The Representative static PET imaging of ^{11}C-FAPI-02 at 30, 60, 90min in U87MG tumor-bearing nude mice. And the tumor was indicated by the red circle; **b**: The organs or tissues uptakes of ^{11}C-FAPI-02 in U87MG tumor-bearing nude mice at 30, 60, 90min; **c**: the time-active-curve (TAC) of ^{11}C-FAPI-02 at 30, 60, 90min.

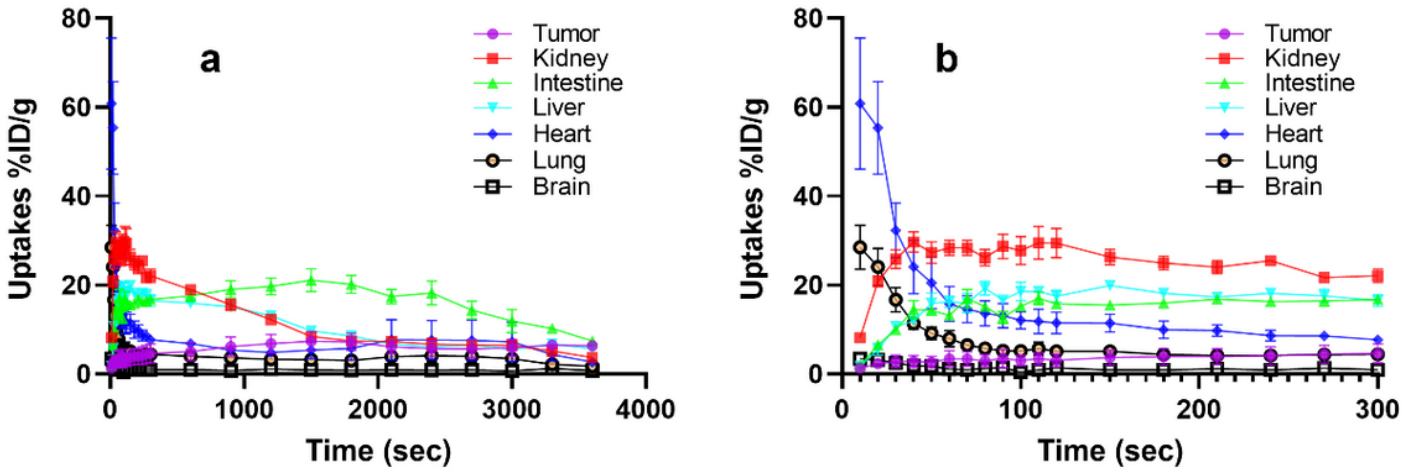

Figure 5

Dynamic time-activity curves of ^{11}C-FAPI-02 in the heart, kidney, liver, brain, lung, Intestine, and tumor in U87MG tumor-bearing nude mice. the difference between **a** and **b** is the ordinate, for **a** the time is from 0 to 3600 seconds. And for **b** the time is from 0 to 300 seconds.

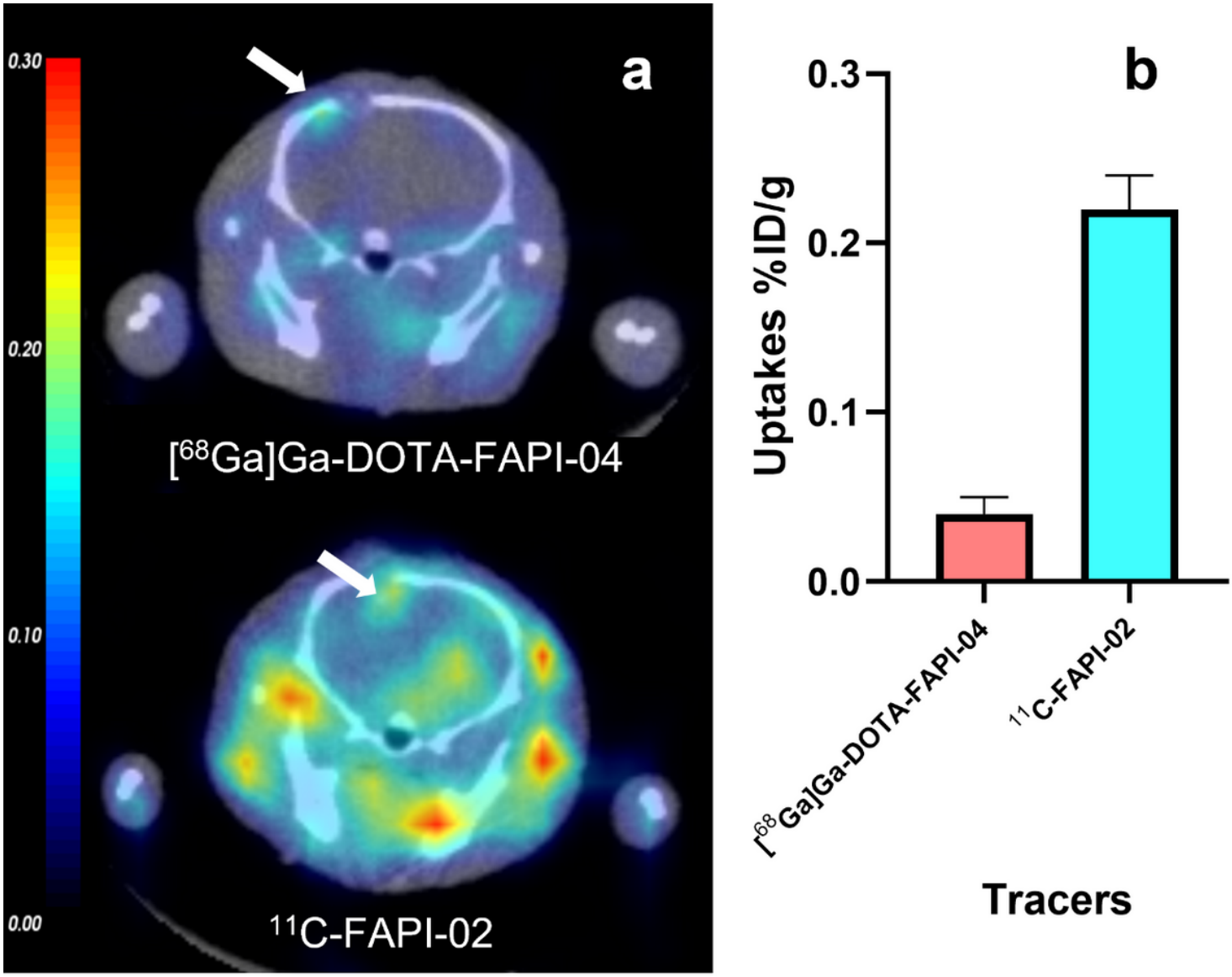

Figure 6

The orthotopic xenograft gliomas model small animal PET of ^{11}C-FAPI-02 and [^{68}Ga]Ga-DOTA-FAPI-04 at 60min p.i.. **a**: The representative static PET imaging of ^{11}C-FAPI-02 and [^{68}Ga]Ga-DOTA-FAPI-04 at 60min p.i. in U87MG orthotopic xenograft gliomas models. **b**: The uptakes of ^{11}C-FAPI-02 and [^{68}Ga]Ga-DOTA-FAPI-04 in tumor.

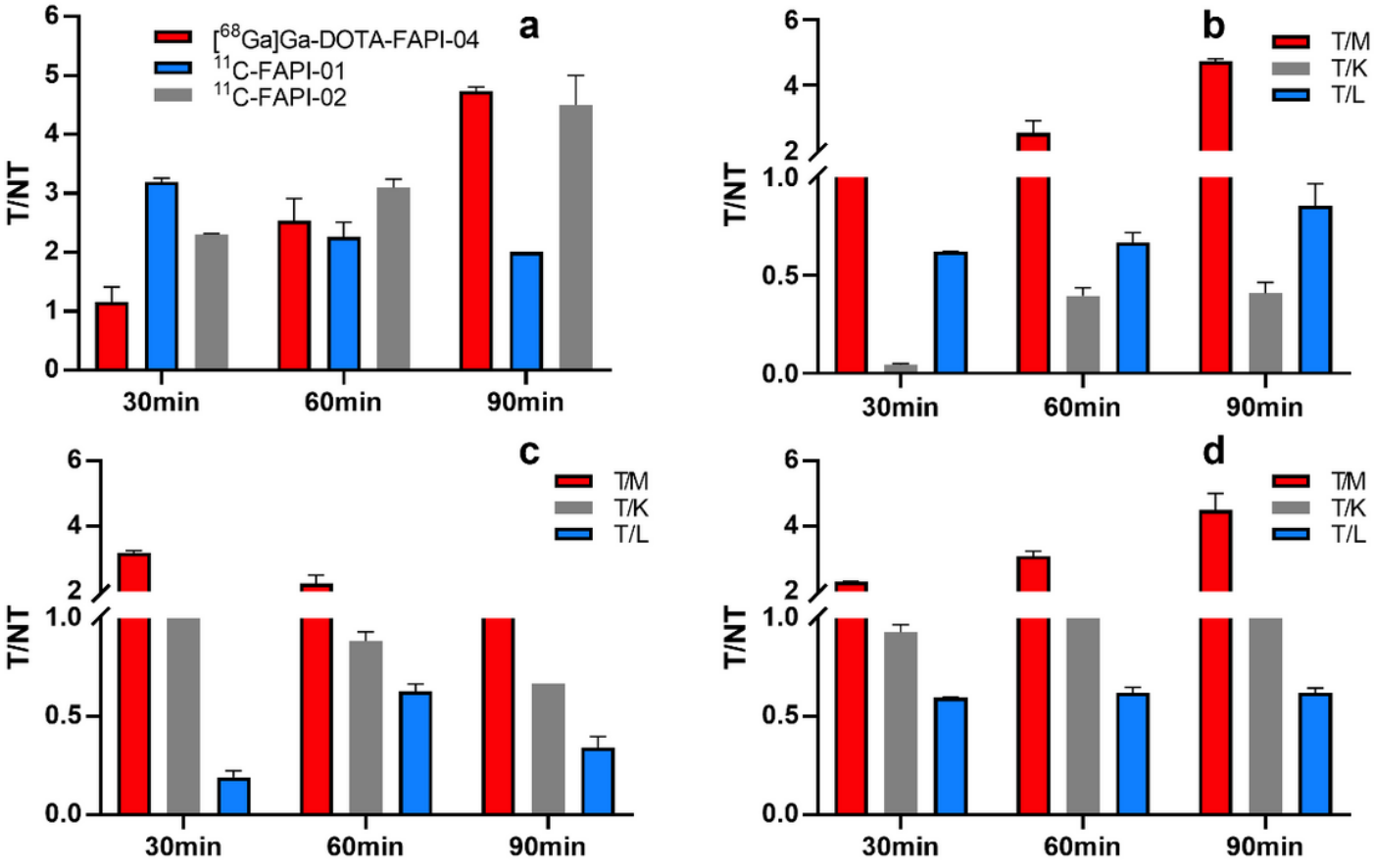

Figure 7

The T/NT ratios in U87MG tumor-bearing nude mice of [^{68}Ga]Ga-DOTA-FAPI-04, ^{11}C-FAPI-01, and ^{11}C-FAPI-02. **a**: the T/M ratios of [^{68}Ga]Ga-DOTA-FAPI-04, ^{11}C-FAPI-01 and ^{11}C-FAPI-02 after 30, 60 and 90min p.i.. **b**: the T/M, T/K, and T/L ratios of [^{68}Ga]Ga-DOTA-FAPI-04 after 30, 60 and 90min p.i.. **c**: the T/M, T/K, and T/L ratios of ^{11}C-FAPI-01 after 30, 60 and 90min p.i.. **d**: the T/M, T/K, and T/L ratios of ^{11}C-FAPI-02 after 30, 60 and 90min p.i..

Supplementary Files

This is a list of supplementary files associated with this preprint. Click to download.

- Supplementalmaterials.docx